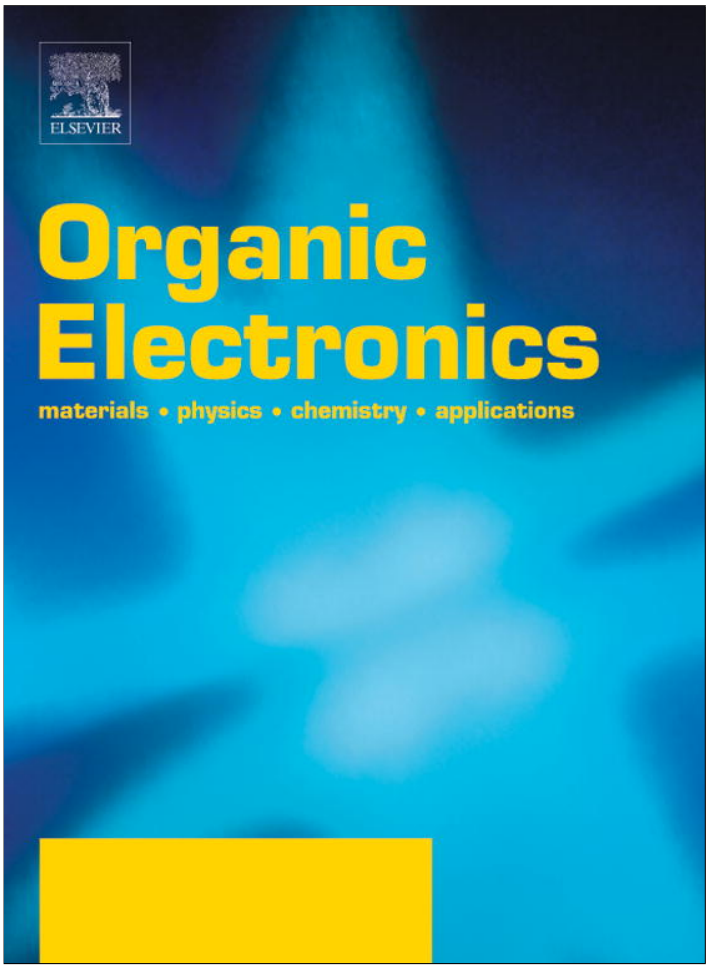

Organic Electronics 14 (2013) 1262–1270

Contents lists available at SciVerse ScienceDirect

Organic Electronics

journal homepage: www.elsevier.com/locate/orgel

Adhesion properties of inverted polymer solarcells: Processing and film structure parameters

Stephanie R. Dupont [a], Eszter Voroshazi [b,c], Paul Heremans [b,c], Reinhold H. Dauskardt [a,*]

[a] Department Materials Science and Engineering, Stanford University, Stanford, CA, USA
[b] IMEC vzw, Leuven, Belgium
[c] ESAT, KULeuven, Leuven, Belgium

ARTICLE INFO

Article history:
Received 6 November 2012
Received in revised form 9 February 2013
Accepted 16 February 2013
Available online 6 March 2013

Keywords:
Adhesion and delamination in thin film structures
Reliability
P3HT:PCBM inverted polymer solar cells
PEDOT:PSS and MoO_3
Processing parameters

ABSTRACT

We report on the adhesion of weak interfaces in inverted P3HT:PCBM-based polymer solar cells (OPV) with either a conductive polymer, PEDOT:PSS, or a metal oxide, molybdenum trioxide (MoO_3), as the hole transport layer. The PEDOT:PSS OPVs were prepared by spin or spray coating on glass substrates, or slot-die coating on flexible PET substrates. In all cases, we observed adhesive failure at the interface between the P3HT:PCBM with PEDOT:PSS layer. The adhesion energy measured for the solar cells made on glass substrates was about 1.8 J/m^2, but only 0.5 J/m^2 for the roll-to-roll processed flexible solar cells. The adhesion energy was insensitive to the PEDOT:PSS layer thickness in the range of 10–40 nm. A marginal increase in adhesion energy was measured with increased O_2 plasma power. Compared to solution processed PEDOT:PSS, we found that thermally evaporated MoO_3 adheres less to the P3HT:PCBM layer, which we attributed to the reduced mixing at the MoO_3/P3HT:PCBM interface during the thermal evaporation process. Insights into the mechanisms of delamination and the effect of different material properties and processing parameters yield general guidelines for the design of more reliable organic photovoltaic devices.

1. Introduction

Organic photovoltaic (OPV) devices typically involve materials that are compatible with flexible plastic substrates resulting in light-weight and decorative products using inexpensive roll-to-roll (R2R) module fabrication [1–3]. Current state-of-the-art OPVs have reached over 10% power conversion efficiency (PCE), one of the critical milestones for market introduction [4], although they remain limited in size. While the electrical failure mechanisms in OPVs have been extensively investigated [5–7], little is known about their mechanical stability, which is an equally important factor determining their reliability during processing and in service. It is well established that the processing yield and the long-term reliability of multilayer electronic devices are strongly influenced by the adhesive and cohesive properties of internal bi-materials and thin films, respectively [8–10]. Adhesive or cohesive failure may result from thin-film strains and associated elastic stresses present in OPVs [11–13]. Differential strains between the OPV layers may arise from shrinkage during solution processing, thermal expansion mismatch, growth from metallization, mechanical handling including flexing and bending, and other operational and environmental forces, such as wind and hail. The resulting mechanical stresses provide the driving force for delamination of weak interfaces or decohesion of weak layers. This leads to a loss of mechanical integrity and device performance.

In this study, we report on the adhesion of weak interfaces in inverted poly(3-hexylthiophene) and

* Corresponding author. Address: Department of Materials Science and Engineering, Stanford University, Stanford, CA 94305-2205, USA. Tel.: +1 650 725 0679; fax: +1 650 725 4034.
E-mail address: dauskardt@stanford.edu (R.H. Dauskardt).

1566-1199/$ - see front matter © 2013 Published by Elsevier B.V.
http://dx.doi.org/10.1016/j.orgel.2013.02.022

1-(3-methoxycarbonyl)-propyl-1-phenyl-(6,6)C_{61} blend (P3HT:PCBM) based polymer solar cells. The critical adhesion or cohesion energy, G_c (J/m^2), is defined as the macroscopic work of fracture per unit area to separate two layers or break a layer, respectively [8]. This property is typically strongly dependent on the material properties, including chemistry and microstructure, mechanical loading mode, and processing conditions. Within a stack of thin films, the crack will usually propagate along the weakest interface or layer, resulting in adhesive or cohesive failure, respectively. A double cantilever beam (DCB) based adhesion technique (Fig. 1) was used to measure the adhesion energy of the interfaces in the inverted OPV structure. This technique is well established and has the advantage of providing quantitative and reproducible measurements, as demonstrated in previous studies [8,14]. The choice of the inverted device architecture is motivated by its intrinsic air stability and compatibility with R2R processing without compromising device efficiency, proving the industrial relevance of this device architecture.

P3HT:PCBM based OPVs with two types of hole transport layers (HTLs) were selected for study. The first HTL is the well known highly conductive polymer poly(3,4-ethylenedioxythiophene) poly(styrene-sulfonate) (PEDOT:PSS). It is widely used as a HTL and also as a transparent electrode in organic electronic devices because of its high visible light transmission combined with elevated conductivity. Additionally, its formulation can be adapted to a variety of printing techniques without a loss of opto-electronic properties. However, due to its hygroscopic nature, PEDOT:PSS loses its mechanical strength and cohesion in humid environments [15,16] and is also subjected to photo-oxidation [17,18]. From a stability point of view, these are the two main reasons why more stable alternatives like metal oxides are being considered [19–21]. The second HTL selected for study was molybdenum trioxide (MoO_3). This metal oxide HTL was compared with our previously reported study of flexible vanadium oxide (V_2O_5) based solar cells [11].

In order to assess the effect of the processing method, the P3HT:PCBM and PEDOT:PSS layers were prepared by spin or spray coating on glass substrates, or R2R slot-die coating on flexible PET substrates. In all cases, we observed adhesive failure at the interface between the P3HT:PCBM and PEDOT:PSS layers. The adhesion energy of this interface was comparable for all the solar cells made on glass substrates, but was lower for the R2R processed flexible solar cells. The adhesion energy was independent of the PEDOT:PSS thickness in the range of 10–40 nm. A marginal increase in adhesion energy was measured with increased O_2 plasma power. Compared to solution processed PEDOT:PSS, we found that thermally evaporated MoO_3 adheres less to the P3HT:PCBM layer. This was most probably due to the reduced mixing with P3HT:PCBM during the thermal evaporation process. Finally, a number of guidelines to improve the fracture properties of P3HT:PCBM-based OPVs will be suggested.

2. Experimental

2.1. Solar cell preparation

The structure of the inverted P3HT:PCBM-based polymer solar cells is shown in Fig. 1. A zinc oxide (ZnO) precursor was deposited from solution onto cleaned indium tin oxide (ITO) coated glass substrates (Kintec). A 250 nm active layer composed of 1:1 wt.% mixture of P3HT:PCBM was deposited from solution. This solution contained as purchased P3HT and PCBM dissolved in o-dichloro-benzene (oDCB) to spin and spray coat the P3HT:PCBM layer, as summarized in Table 1. 1,3,5-trimethylbenzene (mesitylene) was added to the solution for spray coating to favor substrate coverage and reduce surface roughness. Note that in the case of the R2R processed flexible OPVs, P3HT and PCBM were dissolved in chloro-benzene (CB) to slot-die coat the P3HT:PCBM layer. Prior to thermal evaporation of the silver electrode (Ag, 100 nm), a thin HTL was deposited. The HTL was either a solution processed PEDOT:PSS layer or a thermally evaporated 30 nm MoO_3 layer. The PEDOT:PSS layer was deposited from a commercially available water-based dispersion (Baytron PVP AI 4083 or EL-P 5010) selectively diluted by isopropanol (IPA) and deionized water (DIW) as summarized in Table 1. Spin coated PEDOT:PSS layers with different thicknesses were deposited by systematically varying the spin coating velocity. A 60 s oxygen (O_2) plasma treatment on the spin and spray coated P3HT:PCBM layers prior to PEDOT:PSS deposition was used to enhance the wettability of PEDOT:PSS solution with the plasma power (kW), the spin coating velocity (rpm) and corresponding layer thickness (nm) reported in Table 2. Further details on the processing on glass substrates [18,19] and the R2R processing on flexible polyethylene terephthalate substrates [20] have been previously reported.

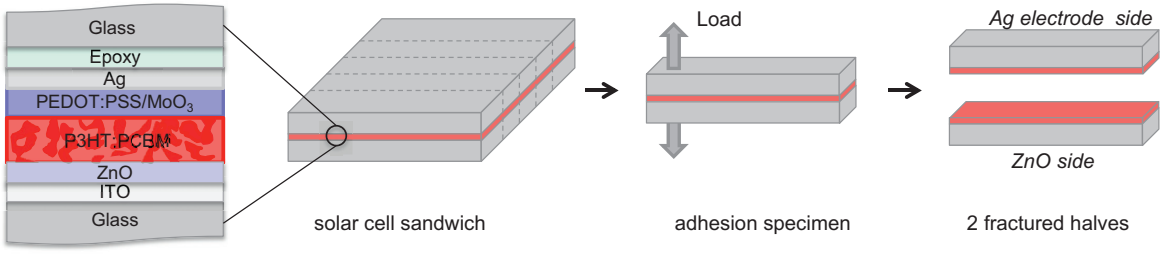

Fig. 1. Illustration of the solar cell structure and the square glass sandwich. With a wafer saw, 2 identical DCB adhesion specimens are cut out. After adhesion testing, 2 fractured halves are obtained and referred to as the Ag electrode side and the ZnO side.

Table 1
For the different processing methods, the product name and manufacturer of the materials, the solvents, and possible additives used in the solution are given.

Organic layer	Processing method	Product name/manufacturer	Solvents and additives
P3HT:PCBM	Spin coating	P3HT: Rieke Materials PCBM: Solenne B.V.	oDCB
	Spray coating	P3HT: Rieke 4002-EE PCBM: Solenne B.V.	70 vol.% oDCB 30 vol.% mesitylene
	Slot-die coating	P3HT: Sepiolid P200, BASF PCBM: Solenne B.V.	CB
PEDOT:PSS	Spin coating Spray coating	Baytron P VP AI 4083: Clevios Baytron PVP AI 4083: Clevios	100 vol.% PEDOT:PSS 73 vol.% IPA 18 vol.% PEDOT:PSS 9 vol.% DIW
	Slot-die coating	EL-P 5010: Agfa	IPA PEDOT:PSS

Table 2
The G_c and PCE values for samples with different PEDOT:PSS layer thicknesses and the corresponding spin coating velocities. The power of the plasma treatment (60 s) before deposition of PEDOT:PSS is given in the first column.

Sample	Power plasma treatment (kW)	Spin coating velocity of PEDOT:PSS (RPM)	Thickness PEDOT:PSS, t (nm)	Adhesion energy, G_c (J/m^2)	PCE (%)
1	100	5000	10	1.34 ± 0.05	3.10
2	180	5000	10	1.59 ± 0.08	3.24
3	100	4000	20	1.22 ± 0.06	3.20
4	100	2000	40	1.53 ± 0.11	3.25

2.2. Adhesion specimen

An identical glass substrate was bonded on top of the silver electrode using a brittle epoxy (Fig. 1) resulting in a square glass sandwich. From this sandwich, rectangular double cantilever beam adhesion specimens of 5 mm wide, 30 mm long and 1.5 mm thick were machined using a high speed wafer saw with a resin blade. To prevent water coolant from diffusing into the solar cell structure during dicing and thereby damaging the solar cell materials, trenches were cut on each side of the square sandwich. Perfectly aligned trenches on the top and bottom glass beam made it easy to cleave individual adhesion specimens prior to testing.

2.3. Thin-film adhesion testing

The adhesion specimens were loaded under displacement control in a thin-film adhesion testing system (Delaminator DTS, Menlo Park, CA) from which a load, P, versus displacement, Δ, curve was recorded. The adhesion energy, G_c (J/m^2), was measured in terms of the critical value of the applied strain energy release rate. G_c can be expressed in terms of the critical load, P_c, at which crack growth occurs, the crack length a, the plain strain elastic modulus, E', of the substrates and the specimen dimensions; width, b and half- thickness, h. The adhesion energy was calculated from Eq. (1) [22]:

$$G_c = \frac{12P_c^2a^2}{B^2E'h^3}\left(1 + 0.64\frac{h}{a}\right)^2 \quad (1)$$

The crack length was measured directly under an optical microscope and also inferred from measurement of the elastic compliance, $d\Delta/dP$, using the following compliance relationship:

$$a = \left(\frac{d\Delta}{dP} \times \frac{BE'h^3}{8}\right)^{1/3} - 0.64 \times h \quad (2)$$

All testing was carried out in laboratory air environment at ~25 °C and ~40% relative humidity.

2.4. Surface characterization

Following mechanical testing, a survey X-ray photo spectroscopy (XPS, PHI 5000 Versaprobe) scan (0–1000 eV) was made on the debonded surfaces using monochromatic Al Kα X-ray radiation at 1487 eV in order to characterize the surface chemistry and to help precisely locate the debond path. Detailed high-resolution XPS scans were made in regions of spectra containing peaks of interest for additional compositional analysis. Contact angles (CA) (190, rame-hart) were measured with ethylene glycerol (ACROS Organics, 99+%) to further quantify the debond surface chemistry. Atomic force microscopy (AFM) (XE-70, Park Systems) was used to characterize the surface morphology and roughness in a non-contact mode.

3. Results and discussion

3.1. Adhesion of the P3HT:PCBM/PEDOT:PSS interface

The effect of processing methods on G_c and PCE of inverted solar cells prepared by spin or spray coating on glass substrates is shown in Fig. 2. To complement the study, results from a previously published study on flexible

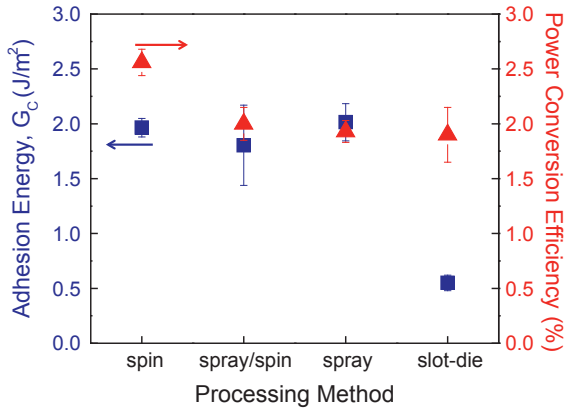

Fig. 2. The adhesion energy, G_c (J/m^2) (■) and the PCE (▲) as a function of various processing methods. Spin, Spray and Slot-Die refers to the processing method of both the P3HT:PCBM and the PEDOT:PSS layers, while Spray/Spin refers to a spray coated P3HT:PBM layer and a spin coated PEDOT:PSS.

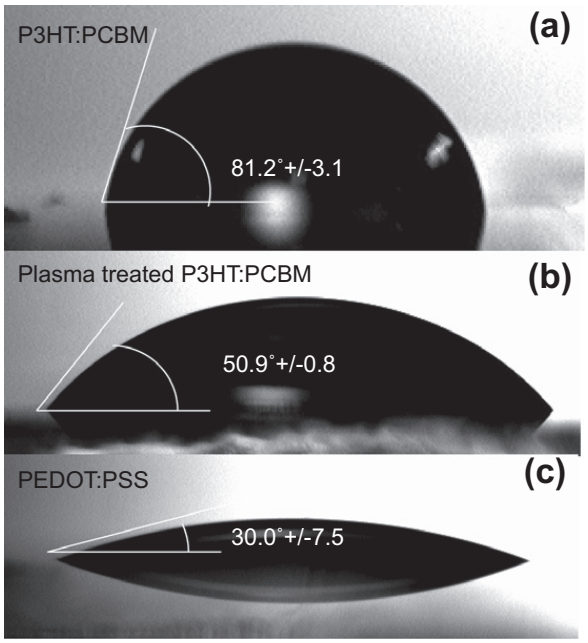

Fig. 3. A drop of ethylene glycol making different contact angles on top of the reference layers; (a) P3HT:PCBM, (b) O_2 plasma treated P3HT:PCBM and (c) PEDOT:PSS.

inverted polymer solar cells, in which the layers of interest were slot-die coated [11], are also shown on the figure. The P3HT:PCBM/PEDOT:PSS was the weakest interface in all cases [13]. G_c ranged from ~1.7 to 2 J/m^2 for all the OPVs on glass substrates, but was only 0.5 J/m^2 for the flexible slot-die coated OPVs. This is most probably due to morphological and structural organization, and interfacial chemistry, even though XPS resolved no significant differences between the samples. For the different processing methods, the PEDOT:PSS and P3HT:PCBM layers were processed from different solutions (Table 1). This affects the interaction between both layers, during and after deposition and affects the adhesion between those two organic layers. The flexible OPVs were also fully processed in air. Impurities like water, hydrogen, and oxygen can either diffuse into or attack the materials, and thereby affect the interfacial chemistry and thus the adhesion properties. Note that in this work we have consistently compared OPVs with analogous PCEs in the range of 2–2.5%.

To further elucidate the failure path, ethylene glycerol contact angels (CAs) of the reference layers and the fractured surfaces were measured and listed in Table 3. The reference CA of as-deposited P3HT:PCBM, O2 plasma treated P3HT:PCBM and PEDOT:PSS were 81.2° ± 3.1, 50.9° ± 0.8, and 30.0° ± 7.5, respectively (Fig. 3). The fracture surface CA on the Ag electrode side varied between 29° and 34°, which corresponded to the CA of PEDOT:PSS. Similarly, the CA on the ZnO side varied between 81° and 84°, indicative of the P3HT:PCBM layer. The CA of the delaminated P3HT:PCBM layer was the same as the untreated reference layer, indicating the temporary result of a O_2 plasma treatment, which was used to make the surface less hydrophobic, hence improving the wetting by PEDOT:PSS. The CA measurements clearly indicated adhesive failure at the P3HT:PCBM/PEDOT:PSS interface.

Detailed XPS characterization revealed about 85–90 at.% carbon (C), 6–8 at.% sulfur (S) and 3.5–10 at.% oxygen (O) on the Ag electrode side and 90–95 at.% C, 4.5–7 at.% S and 0–3 at.% O on the opposite ZnO side (see supplementary information). High resolution S_{2p} scans revealed one peak around 164 eV, corresponding to single sulfur–oxygen bonds and/or single sulfur–carbon bonds, and a second peak around 168 eV corresponding to double sulfur–oxygen bonds. The 164 eV peak was observed at both cleaved surfaces, whereas the 168 eV peak was only apparent at the Ag electrode side or PEDOT:PSS interface, corresponding to the sulfonic acid group in PSS. XPS measurements indicated adhesive failure at the P3HT:PCBM/PEDOT:PSS interface [23,24]. In conclusion, both XPS and CA measurements revealed adhesive failure between the P3HT:PCBM and PEDOT:PSS layers.

AFM was used to characterize the surface roughness of the spin and spray coated P3HT:PCBM and PEDOT:PSS layers and to study their effect on the adhesion properties.

Table 3
The measured contact angles of the reference samples and the surfaces of the two fractured specimens; Ag electrode side and ZnO side of X/Y Coated P3HT:PCBM, PEDOT:PSS respectively.

Reference sample	Contact angle (Θ_c)	Sample	Contact angle (Θ_c)	
		P3HT:PCBM/PEDOT:PSS	Ag electrode side	ZnO side
P3HT:PCBM	81.2° ± 3.1	Spin/Spin	33.8°	81.2°
Plasma P3HT:PCBM	50.9° ± 0.8	Spray/Spin	33.2°	83.3°
PEDOT:PSS	30.0° ± 7.5	Spray/Spray	29.0°	81.2°

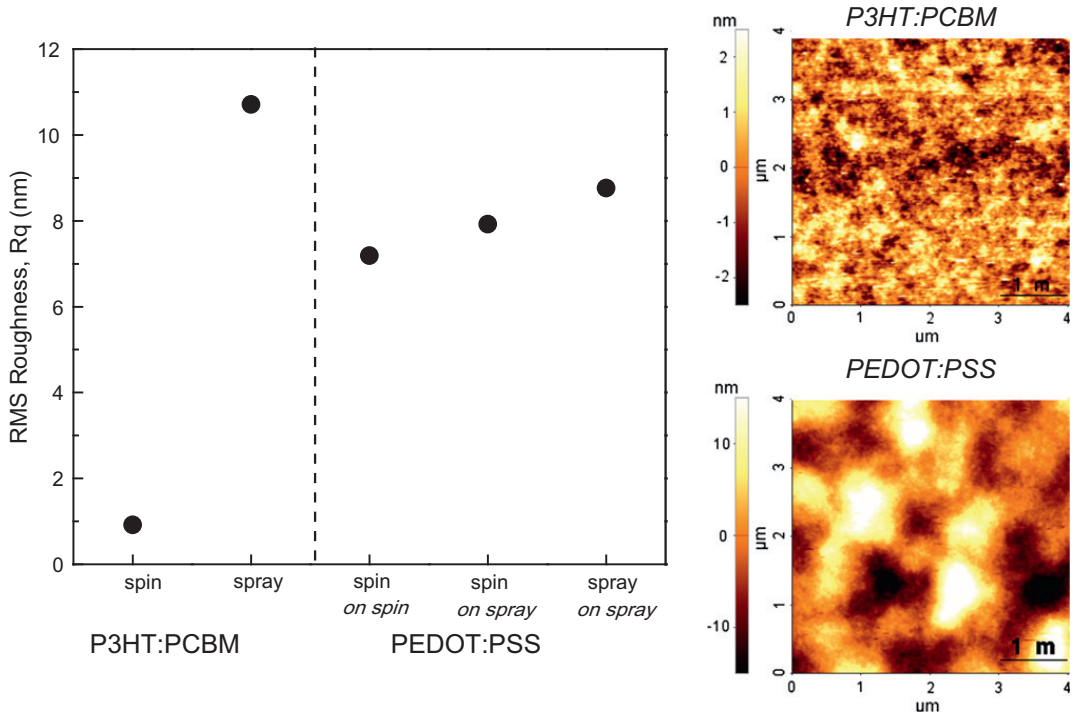

Fig. 4. (a) The measured root-mean square roughness (R_q, nm) of spin coated P3HT:PCBM , spray coated P3HT:PCBM, spin coated PEDOT:PSS on top of a spin coated P3HT:PCBM, spin coated PEDOT:PSS on top of spray coated P3HT:PCBM and spray coated PEDOT:PSS on top of spray coated P3HT:PCBM is presented. (b) 4 μm × 4 μm AFM images of spin coated P3HT:PCBM and (c) spin coated PEDOT:PSS. The scale bar represents 1 μm.

AFM surface scans of these organic layers were taken over a 4 μm × 4 μm area and the measured root-mean square roughness (R_q, nm) is shown in Fig. 4. The spin coated P3HT:PCBM layer (R_q of 0.92 nm) had a much smoother surface than the spray coated one (R_q of 10.71 nm). The spin and spray coated PEDOT:PSS layers smoothed the spray coated P3HT:PCBM layer with an R_q in the range of 8–9 nm. Despite the large surface roughness difference between the spin and spray coated P3HT:PCBM and the use of mesitylene (Table 1) to prepare the spray coated layer, there was no measured effect in terms of G_c values, as described earlier.

In normal device geometries, cohesive failure in the P3HT:PCBM layer was observed [12]. In the present inverted device geometries, adhesive interfacial failure is observed (Fig. 5). This indicates that the P3HT:PCBM/PEDOT:PSS interface was stronger for normal device geometries and, consequently, the crack had propagated cohesively in the P3HT:PCBM layer. The weak P3HT:PCBM/PEDOT:PSS interface in the inverted device geometries may be related to a number of factors. One involves poor wetting of the hydrophilic PEDOT:PSS solution on the hydrophobic P3HT:PCBM film during processing, suggesting reduced chemical interaction between the two organic layers and a lower resulting adhesion.

Another factor may be related to the vertical phase separation observed in both the P3HT:PCBM [25–28] and PEDOT:PSS layers [23,29]. In the PEDOT:PSS layer, a PEDOT-rich region is found at the bottom and a PSS-rich region is found towards the top surface interface with air during deposition. In the normal device geometry, P3HT:PCBM is deposited on top of the PEDOT:PSS layer (Fig. 5a) and a P3HT-rich region develops towards the bottom of the layer near the interface with the PEDOT:PSS. P3HT and PSS can physically intermix and electrochemically react to form a strong $P3HT^+$:PSS^- interface layer [30]. However, in the inverted device geometry, the P3HT:PCBM layer is first deposited on top of the ZnO electrode (Fig. 5b). Due to the induced dipole–dipole interaction between ZnO and PCBM, a PCBM-rich region is now developed towards the bottom of the film at the ZnO interface. At the same time, the lower surface energy polymer P3HT tends to segregate to the top of the film and the interface with air. When the PEDOT:PSS layer is deposited on top of the P3HT:PCBM, the P3HT-rich top region is in direct contact with the PEDOT-rich and PSS-depleted region. The formation of the strong $P3HT^+$:PSS^- interface layer, as seen in the normal device geometry, is reduced. This results in a weak adhesion between the PEDOT:PSS and P3HT:PCBM layers in the inverted geometry.

To assess the effect of the PEDOT:PSS layer thickness, several OPVs processed under identical conditions, differing only in thickness, were studied. G_c values of 1.4 ± 0.2 J/m^2 were measured for the P3HT:PCBM/PEDOT:PSS interface with PEDOT:PSS film thickness ranging from 10 nm to 40 nm (Table 2). We observed little effect of the polymer layer thickness on both the G_c and PCE values. Previous research has shown that the cohesion of P3HT:PCBM was also insensitive to the P3HT:PCBM layer thickness [12]. These are surprising results, since the adhesion or cohesion of polymeric thin films often has a strong dependence on film thickness [31]. The contribution to G_c from energy dissipation through the formation of a plastically deformed zone at the crack tip when fracture occurs,

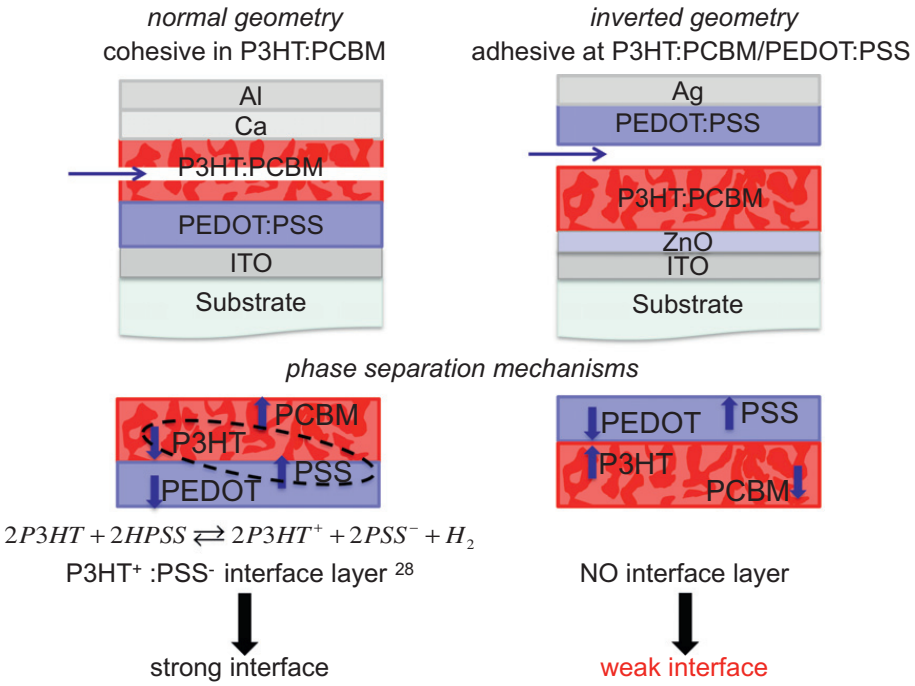

Fig. 5. Schematic of the normal and inverted geometry, showing the difference in failure path. Cohesive failure in the P3HT:PCBM and adhesive failure at the P3HT:PCBM/PEDOT:PSS interface. Phase Separation explains the presence of a strong $P3HT^{+}$:PSS^{-} interface in normal device geometry and the absence of this strong interface in the inverted geometry.

or adjoint to, an elastic–plastic polymeric film is a significant and well-studied phenomenon [32–34]. The P3HT:PCBM has mechanical properties that are very similar to the PEDOT:PSS layer [35]. The plastic zone size formed ahead of a crack tip at this interface would spread into the both the P3HT:PCBM and PEDOT:PSS layers and would only be constrained by the strong and yielding resistant ZnO and Ag layers. In the case of a constrained plastic zone, the plastic zone size is expected to increase with the polymer thickness and consequently, G_c is expected to increase. Since we do not observe any dependence of thickness on G_c, we can conclude that these films have little crack tip plasticity and the plastic zone size is always smaller than the combined polymer film thicknesses.

The effect of the O_2 plasma treatment power prior to PEDOT:PSS deposition is briefly studied here. A marginal increase in adhesion energy was observed with increased plasma power. The G_c was measured to be 1.34 J/m^2 for the sample treated at 100 kW (#1 in Table 2) and 1.59 J/m^2 for the sample treated at 180 kW (#2 in Table 2). Higher plasma power generally resulted in a rougher surface, as well as a decreased hydrophobicity and an increased wettability [36,37]. This improves the molecular interactions between the PEDOT:PSS and P3HT:PCBM layers and could explain the observed increase in adhesion with increased plasma power during the O_2 plasma treatment.

3.2. Adhesion of P3HT:PCBM/MoO_3 interface

The adhesion energy of the P3HT:PCBM with MoO_3 interface was measured to be 0.85 ± 0.15 J/m^2, shown in Fig. 6. The fracture surface CA on the Ag electrode side was measured 20.3 ± 1.6, which corresponded to the CA

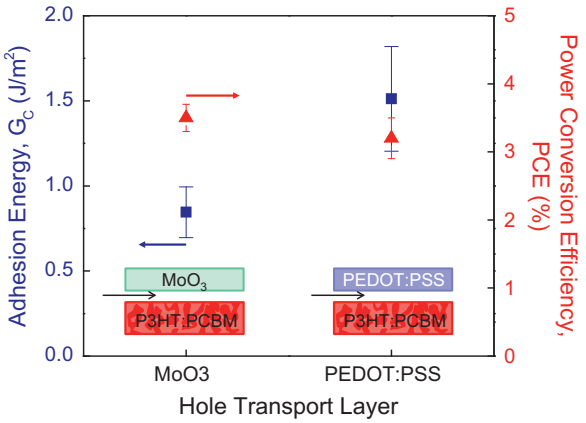

Fig. 6. The adhesion energy, G_c (J/m^2) (■) and the PCE (▲) for inverted P3HT:PCBM-based polymer solar cells with either MoO_3 or PEDOT:PSS as the hole transport layer. Adhesive failure occurred at the HTL/P3HT:PCBM interface.

of MoO_3. Similarly, the CA on the ZnO side was measured 83° ± 2.5, indicative of the P3HT:PCBM layer. XPS characterization of the broken fracture surfaces revealed 74.17 at.% C, 5.22 at.% S, 14.53 at.% O, 5.56 at.% molybdenum (Mo), and 0.42 at.% Ag at the Ag electrode side and 97.31 at.% C, 7.09 at.% S and 1.61 at.% O at the ZnO side. The CA and XPS measurements together clearly indicated adhesive failure at the P3HT:PCBM/MoO_3 interface.

While the adhesion between the thermally evaporated metal oxide MoO_3 and P3HT:PCBM layers is much lower than the adhesion between PEDOT:PSS and P3HT:PCBM layers, we have previously shown that adhesion between a solution processed vanadium oxide (V_2O_5) and P3HT:PCBM layer is significantly higher [11]. Thus, it

would be wrong to conclude that the adhesion with a metal oxide HTL is generally lower than with a polymeric HTL. In contrast, the adhesion is influenced by the chemical interaction and physical interface mixing, which is partly determined by the processing method. Both the PEDOT:PSS and V_2O_5 HTLs were solution processed, involving a solvent that allows physical intermixing at the interface and promoting the formation of a strong interfacial layer. The MoO_3 layer was deposited by thermal evaporation, a deposition method not involving a solvent that enables physical interface mixing with the underlying layer. It is well known that physical vapor deposited metal oxides cause degradation to the underlying organic layer [38–40]. The absence of a substantial mixed interface layer and the degradation caused by evaporation are both responsible for the observed weaker adhesion between the P3HT:PCBM and MoO_3 layers.

4. Guidelines

The fracture properties (adhesion and cohesion) of OPVs are determined by the composition and processing conditions of the individual OPV layers. These determine the key interfacial and film parameters, such as interface chemistry, bonding, impurity content, morphology and adjoining nanostructure. In this section, we summarize how the fracture properties can be improved by tuning film parameters, such as the thickness and composition, and processing steps (annealing and processing method) along with pre-deposition treatments and adhesion promoters.

4.1. Organic layer thickness

The adhesion energy of the P3HT:PCBM/PEDOT:PSS interface and the cohesion energy of the P3HT:PCBM layer [12] have to date been found largely insensitive to the polymer film thickness. However, generally the adhesion and/or cohesion of polymer films have a strong dependence on the film thickness due to energy dissipation through plastic or viscoelastic deformation that occurs near to the crack tip in the polymer layer. For example, in poly(arylene) films [31], film thickness cohesion depencence was observed over a wide range of thicknesses to as low as 5 nm. The thickness independent fracture properties for current P3HT:PCBM OPVs is related to their relatively weak intermolecular layers and little or no attendant plasticity [12]. The extent of plastic deformation in the PEDOT:PSS also appears limited, at least over the range explored in the present study. However, ongoing research efforts have shown that higher molecular weight P3HT:PCBM layers exhibit much higher G_c values due to the greater degree of molecular entanglement and interactions. These lead to plastic or viscoelastic energy dissipation and an opportunity to tune film thicknesses to achieve significant improvements in fracture resistance.

4.2. Composition

The polymer:fullerene (P3HT:PCBM) ratio has a significant impact on both the cohesion of the P3HT:PCBM layer and the adhesion with the adjacent PEDOT:PSS layer [11,12]. The adhesion with PEDOT:PSS was the greatest for a pure P3HT layer and reduced with increasing PCBM wt.%. The cohesion of the P3HT:PCBM layer was again the lowest for a pure PCBM, increased with P3HT wt.%, and reached a maximum at 75 wt.% P3HT. Fullerene-rich layers clearly lead to mechanically weak layers with low adhesion and cohesion.

4.3. Annealing

Annealing is widely used to induce phase separation in the P3HT:PCBM layer and enhance polymer crystallization, which improves charge transport and device efficiency. But, it also changes the interface chemistry, bonding, and morphology, which in turn affects the fracture properties. Our studies generally reveal that annealing can enhance both the cohesive properties of the P3HT:PCBM layer and the adhesive properties of the P3HT:PCBM/PEDOT:PSS interface. Optimized annealing conditions are dependent on the specific molecules and their molecular weight, and fine tuning of the anneal process for the best combination of PCE, in-service thermal stability, and fracture resistance should be performed.

4.4. Processing method

The adhesion between the P3HT:PCBM and the HTL is greatly influenced by the processing method, since it determines the degree of interface intermixing and entanglement. Solution processed methods, such as spin, spray, and slot die coating, involve a solvent which allows physical intermixing at the interface. For example, it is shown that a solution processed V_2O_5 HTL formed a very strong 10 nm thick interfacial layer with the P3HT:PCBM [11]. In PEDOT:PSS-based normal device geometry OPVs, the P3HT polymers and PSS polymers from the HTL physically intermix and electrochemically react to form a strong $P3HT^+$:PSS^- interface layer up to a few nm thick. On the other hand, deposition by thermal evaporation does not involve such a solvent. The evaporation process results in less physical interface mixing, reduced molecular interactions, and therefore weaker adhesion. Other processing parameters such as the coating solvent, solution concentration, and the drying time can also have a great influence on the morphology and the interfacial chemistry of the P3HT:PCBM layer [41] and should therefore be tuned accordingly to achieve high fracture resistance.

4.5. Pre-deposition treatments and adhesion promotors

To improve the wetting of hydrophilic PEDOT:PSS solution on the hydrophobic P3HT:PCBM film, surface treatments are generally applied. For example, in this work O_2 plasma treatment prior to PEDOT:PSS deposition was used. A marginal increase in adhesion was found with increased plasma power. However, treatments and surfactants designed for improved wettability do not always result in better adhesion. To improve adhesion, the chemical interaction between adjacent layers must be improved and if possible the two layers should physically intermix at the

interface. This can be achieved in several ways. Surface activation of the underlying layer can be used. For example, O_2 plasma treatment with the addition of a few percentages of CF_4 can provide extra reactivity to the surface [42]. Solvation can soften the surface of the polymer layer and thereafter increase the degree of intermixing between the two polymer layers. Microgels, such as poly(allylamine hydrochloride) and dextran (PAH-D), can be used as an adhesive interlayer [43]. The PAH-D interfacial layer is expected to improve the adhesion due to the hydrophobic/hydrophobic interactions between P3HT:PCBM and PAH-D at one side and the electrostatic interactions formed between the ionic groups on the PAH-D and PSS on the other side. Finally, an ink can be engineered that improves PEDOT:PSS wetting and allows deeper penetration in the P3HT:PCBM.

5. Conclusions

The effect of processing method, layer thickness, O_2 plasma power, and HTL on the adhesion properties in inverted P3HT:PCBM-based polymer solar cells (OPV) has been quantified and studied. For the PEDOT:PSS-based solar cells, the P3HT:PCBM/PEDOT:PSS interface was found to be the weakest with adhesion energy values ranging from 0.5 to 2 J/m^2, depending on the processing method. Little effect of the PEDOT:PSS layer thickness on the adhesion was observed and a marginal increase in adhesion was measured with O_2 plasma power. MoO_3 adheres considerably less to P3HT:PCBM than PEDOT:PSS, due to the reduced physical mixing involved in a thermal evaporated process compared to a solution process. Based on the observation described in the current and previously reported papers, a number of guidelines to improve the fracture properties of polymer OPVs were suggested.

Acknowledgements

We acknowledge C. Girotto for his assistance with the spray coated sample preparation. This research was supported by the Center for Advanced Molecular Photovoltaics (CAMP) supported by King Abdullah University of Science and Technology (KAUST) under award no. KUS-C1-015-21. S.R. Dupont acknowledges financial support as a fellow of the Belgian American Educational Foundation (B.A.E.F).

Appendix A. Supplementary material

Supplementary data associated with this article can be found, in the online version, at http://dx.doi.org/10.1016/j.orgel.2013.02.022.

References

[1] G. Dennler, M.C. Scharber, C.J. Brabec, Polymer–fullerene bulk-heterojunction solar cells, Adv. Mater. 21 (2009) 1323–1338.
[2] C.J. Brabec, S. Gowrisanker, J.J.M. Halls, D. Laird, S.J. Jia, S.P. Williams, Polymer–fullerene bulk-heterojunction solar cells, Adv. Mater. 22 (2010) 3839–3856.
[3] F.C. Krebs, Fabrication and processing of polymer solar cells: a review of printing and coating techniques, Solar Energy Mater. Solar C 93 (2009) 394–412.
[4] K.E.M.A. Green, Y. Hishikawa, W. Warta, E.D. Dunlop, Solar cell efficiency tables (Version 39), Prog. Photovolt.: Res. Appl. 20 (2012) 12–20.
[5] M. Jorgensen, K. Norrman, F.C. Krebs, Stability/degradation of polymer solar cells, Solar Energy Mater. Solar C 92 (2008) 686–714.
[6] E. Voroshazi, B. Verreet, T. Aernouts, P. Heremans, Long-term operational lifetime and degradation analysis of P3HT: PCBM photovoltaic cells, Solar Energy Mater. Solar C 95 (2011) 1303–1307.
[7] C.H. Peters, I.T. Sachs-Quintana, J.P. Kastrop, S. Beaupre, M. Leclerc, M.D. McGehee, High efficiency polymer solar cells with long operating lifetimes, Adv. Energy Mater. 1 (2011) 491–494.
[8] R. Dauskardt, M. Lane, Q. Ma, N. Krishna, Adhesion and debonding of multi-layer thin film structures, Eng. Fract. Mech. 61 (1998) 141–162.
[9] S.Y. Kook, J.M. Snodgrass, A. Kirtikar, R.H. Dauskardt, Adhesion and reliability of polymer/inorganic interfaces, J. Electron. Packag. 120 (1998) 328–335.
[10] B.M. Sharratt, L.C. Wang, R.H. Dauskardt, Anomalous debonding behavior of a polymer/inorganic interface, Acta Mater. 55 (2007) 3601–3609.
[11] S.R. Dupont, M. Oliver, F.C. Krebs, R.H. Dauskardt, Interlayer adhesion in roll-to-roll processed flexible inverted polymer solar cells, Solar Energy Mater. Solar C 97 (2012) 171–175.
[12] V. Brand, C. Bruner, R.H. Dauskardt, Cohesion and device reliability in organic bulk heterojunction photovoltaic cells, Solar Energy Mater. Solar C 99 (2012) 182–189.
[13] S.R. Dupont, E. Voroshazi, P. Heremans, R.H. Dauskardt The effect of anneal, solar irradiation and humidity on the adhesion/cohesion properties of P3HT:PCBM based inverted polymer solar cells, in: Photovoltaic Specialists Conference (PVSC) 2012 38th IEEE, 2012 pp. 003259–003262.
[14] M.S. Oliver, K.Y. Blohowiak, R.H. Dauskardt, Molecular structure and fracture properties of ZrOX/epoxysilane hybrid films, J. Sol–Gel Sci. Technol. 55 (2010) 360–368.
[15] U. Lang, N. Naujoks, J. Dual, Mechanical characterization of PEDOT:PSS thin films, Synth. Met. 159 (2009) 473–479.
[16] S.R. Dupont, E. Voroshazi, P. Heremans, R.H. Dauskardt Moisture assisted decohesion of PEDOT:PSS conducting films, in progress, 2012.
[17] K. Kawano, R. Pacios, D. Poplavskyy, J. Nelson, D.D.C. Bradley, J.R. Durrant, Degradation of organic solar cells due to air exposure, Solar Energy Mater. Solar C 90 (2006) 3520–3530.
[18] K. Jeuris, L. Groenendaal, H. Verheyen, F. Louwet, F.C. De Schryver, Light stability of 3,4-ethylenedioxythiophene-based derivatives, Synth. Met. 132 (2003) 289–295.
[19] E. Voroshazi, B. Verreet, A. Buri, R. Muller, D. Di Nuzzo, P. Heremans, Influence of cathode oxidation via the hole extraction layer in polymer:fullerene solar cells, Org. Electron. 12 (2011) 736–744.
[20] H.L. Yip, A.K.Y. Jen, Recent advances in solution-processed interfacial materials for efficient and stable polymer solar cells, Energ. Environ. Sci. 5 (2012) 5994–6011.
[21] F.M. Liu, S.Y. Shao, X.Y. Guo, Y. Zhao, Z.Y. Xie, Efficient polymer photovoltaic cells using solution-processed MoO3 as anode buffer layer, Solar Energy Mater. Solar C 94 (2010) 842–845.
[22] M.F. Kanninen, Augmented double cantilever beam model for studying crack-propagation and arrest, Int. J. Fract. 9 (1973) 83–92.
[23] G. Greczynski, T. Kugler, W.R. Salaneck, Characterization of the PEDOT-PSS system by means of X-ray and ultraviolet photoelectron spectroscopy, Thin Solid Films 354 (1999) 129–135.
[24] B.Y. Yu, Y.Y. Chen, W.B. Wang, M.F. Hsu, S.P. Tsai, W.C. Lin, Y.C. Lin, J.H. Jou, C.W. Chu, J.J. Shyue, Depth profiling of organic films with X-ray photoelectron spectroscopy using C(60)(+) and Ar(+) co-sputtering, Anal. Chem. 80 (2008) 3412–3415.
[25] M. Campoy-Quiles, T. Ferenczi, T. Agostinelli, P.G. Etchegoin, Y. Kim, T.D. Anthopoulos, P.N. Stavrinou, D.D.C. Bradley, J. Nelson, Morphology evolution via self-organization and lateral and vertical diffusion in polymer: fullerene solar cell blends, Nat. Mater. 7 (2008) 158–164.
[26] Y. Kim, S. Cook, S.M. Tuladhar, S.A. Choulis, J. Nelson, J.R. Durrant, D.D.C. Bradley, M. Giles, I. Mcculloch, C.S. Ha, M. Ree, A strong regioregularity effect in self-organizing conjugated polymer films and high-efficiency polythiophene: fullerene solar cells, Nat. Mater. 5 (2006) 197–203.
[27] Z. Xu, L.M. Chen, G.W. Yang, C.H. Huang, J.H. Hou, Y. Wu, G. Li, C.S. Hsu, Y. Yang, Vertical phase separation in poly(3-hexylthiophene): fullerene derivative blends and its advantage for inverted structure solar cells, Adv. Funct. Mater. 19 (2009) 1227–1234.
[28] D.S. Germack, C.K. Chan, B.H. Hamadani, L.J. Richter, D.A. Fischer, D.J. Gundlach, D.M. DeLongchamp, Substrate–dependent interface

composition and charge transport in films for organic photovoltaics, Appl. Phys. Lett. 94 (2009).
[29] G. Greczynski, T. Kugler, M. Keil, W. Osikowicz, M. Fahlman, W.R. Salaneck, Photoelectron spectroscopy of thin films of PEDOT-PSS conjugated polymer blend: a mini-review and some new results, J. Electron. Spectrosc. 121 (2001) 1–17.
[30] D.M. Huang, S.A. Mauger, S. Friedrich, S.J. George, D. Dumitriu-LaGrange, S. Yoon, A.J. Moule, The consequences of interface mixing on organic photovoltaic device characteristics, Adv. Funct. Mater. 21 (2011) 1657–1665.
[31] A.V. Kearney, H. Chang, M.E. Mills, R.H. Dauskardt, Influence of porosity and film thickness on adhesion of nanoporous organic dielectrics, in: Advanced Metallization Conference 2006 (AMC 2006), 2007, pp. 517–520.
[32] C.S. Litteken, R.H. Dauskardt, Adhesion of polymer thin-films and patterned lines, Int. J. Fract. 119 (2003) 475–485.
[33] M. Lane, R.H. Dauskardt, A. Vainchtein, H.J. Gao, Plasticity contributions to interface adhesion in thin-film interconnect structures, J. Mater. Res. 15 (2000) 2758–2769.
[34] Y.G. Wei, J.W. Hutchinson, Models of interface separation accompanied by plastic dissipation at multiple scales, Int. J. Fract. 95 (1999) 1–17.
[35] D. Tahk, H.H. Lee, D.Y. Khang, Elastic moduli of organic electronic materials by the buckling method, Macromolecules 42 (2009) 7079–7083.
[36] A. Paproth, K.J. Wolter, R. Deltschew, Adhesion of metal/polymer bonds using PBT, PC, PS and copper, Electr. Comp. C (2006) 959–963.
[37] J.H. Lee, K.S. Hwang, T.S. Kim, J.W. Seong, K.H. Yoon, S.Y. Ahn, Effect of oxygen plasma treatment on adhesion improvement of Au deposited on Pa-c substrates, J. Korean. Phys. Soc. 44 (2004) 1177–1181.
[38] A.V. Walker, T.B. Tighe, B.C. Haynie, S. Uppili, N. Winograd, D.L. Allara, Chemical pathways in the interactions of reactive metal atoms with organic surfaces: vapor deposition of Ca and Ti on a methoxy-terminated alkanethiolate monolayer on Au, J. Phys. Chem. B 109 (2005) 11263–11272.
[39] T. Kugler, M. Logdlund, W.R. Salaneck, Polymer surfaces and interfaces in light-emitting devices, IEEE J. Sel. Top. Quant. 4 (1998) 14–23.
[40] P. Dannetun, M. Logdlund, C. Fredriksson, R. Lazzaroni, C. Fauquet, S. Stafstrom, C.W. Spangler, J.L. Bredas, W.R. Salaneck, Reactions of low work function metals Na, Al, and Ca on alpha, omega-diphenyltetradecaheptaene – implications for metal/polymer interfaces, J. Chem. Phys. 100 (1994) 6765–6771.
[41] H. Hoppe, N.S. Sariciftci, Morphology of polymer/fullerene bulk heterojunction solar cells, J. Mater. Chem. 16 (2006) 45–61.
[42] W.L. Wade, R.J. Mammone, M. Binder, Surface-properties of commercial polymer-films following various gas plasma treatments, J. Appl. Polym. Sci. 43 (1991) 1589–1591.
[43] Q.F. Dong, Y.H. Zhou, J.N. Pei, Z.Y. Liu, Y.W. Li, S.Y. Yao, J.B. Zhang, W.J. Tian, All-spin-coating vacuum-free processed semi-transparent inverted polymer solar cells with PEDOT:PSS anode and PAH-D interfacial layer, Org. Electron. 11 (2010) 1327–1331.